Numerical Analysis of Metal Transfer in Gas Metal Arc Welding

G. WANG, P.G. HUANG, and Y.M. ZHANG

The present article describes a numerical procedure to simulate metal transfer and the model will be used to analyze the transport processes involved in gas metal arc welding (GMAW). Advanced Computational fluid dynamics (CFD) techniques used in this model include a two-step projection method for solving the incompressible fluid flow; a volume of fluid (VOF) method for capturing free surface; and a continuum surface force (CSF) model for calculating surface tension. The electromagnetic force due to the welding current is estimated by assuming several different types of current density distribution on the free surface of the drop. The simulations based on the assumption of Gaussian current density distribution show that the transition from globular to spray transfer mode occurs over a narrow current range and the size of detached drops is nonuniform in this transition zone. The analysis of the calculation results gives a better understanding of this physical procedure. Comparisons between calculated results and experimental results are presented. It is found that the results computed from the Gaussian assumption agree well with those observed in experiments.

I. INTRODUCTION

METAL transfer describes the process of the molten metal movement from the electrode tip to the workpiece in gas metal arc welding (GMAW). A better understanding of the metal transfer process is important for improvements in the quality and productivity of welding. While several distinct modes of the metal transfer have been classified,[1] the globular and spray transfer modes have received attention from many investigations.[1–16] In the globular transfer, the diameter of the drop is much greater than that of the electrode. Spray transfer can be further classified as drop (projected) spray or streaming spray, depending on the diameter of the drop in relation to that of the electrode: approximately the same in drop spray or much smaller in streaming spray. It is found experimentally that a sharp transition in the drop detachment frequency and size occurs when the mode changes between the globular and spray transfer modes. A bifurcation in the drop detachment frequency and the drop size has been observed in the middle of the transition current range.[2,3,4]

A theoretical description of droplet formation in GMAW is complicated by the following effects: the dynamic nature of droplet growth, thermal phenomena in the wire, and heat transfer from the arc. Because of the complexities associated with these effects, models in the literature for prediction of metal transfer in GMAW are typically based on simplified descriptions of the effects influencing the process of droplet formation. The two most well-known models of metal transfer are the static force balance theory (SFBT)[5,6] and the magnetic pinch instability theory (PIT).[7,8] The SFBT considers the balance between gravity, electromagnetic force, plasma drag force, and surface tension. The PIT considers perturbation due to the radial magnetic force acting on an infinite cylindrical column of liquid metal. Nemchinsky[9] developed a steady-state model to describe the equilibrium shape of a pendant droplet with a simple approximation for the current density distribution in the droplet. The preceding models[5–10] are basically static approaches and unable to predict the dynamic behavior of the drop growth during metal transfer. Simpson and Zhu[11] developed a one-dimensional model, which considered the forces acting on the droplet. The model makes the first predictions of droplet shape as a function of time.

Recently, several time-dependent, two-dimensional models have been developed to predict metal transfer. Haider and Lowke[12,13] developed a model for the prediction of droplet formation that included the arc. This model can predict the transition current from the globular to the spray transfer mode in fair agreement with experimental data. In the transition zone between the two modes, the model predicted the presence of both small and large drops. However, the droplet detachment was not addressed and the inclusion of the arc complicated the calculation. The accuracy of computational results is influenced by discontinuity assumptions on the free surface, such as a surface pressure boundary condition. In a recent study by Fan and Kovacevic,[14] the droplet formation, detachment, and transport phenomena are considered together with the weld pool. An approximation was used to get the current density distribution in the droplet by assuming uniform axial current density distribution over horizontal cross section of the droplet. The calculation was carried out only for the globular transfer. Further, Chio *et al.*[15,16] considered the effect of the welding arc under the assumptions of a uniform and linear current density on the droplet surface. The predicted results are in reasonably good agreement with the experimental data, although the transition current is not determined accurately.

Previous models for the prediction of metal transfer have been unable to make accurate predictions of the transition between the globular and spray transfer modes. In this work, a new transient two-dimensional model is developed based on RIPPLE[17] to simulate the droplet formation, detachment, and transport in the globular and spray modes. Wang *et al.*[18,19,20] have successfully conducted numerical analysis for the fluid flow and heat and mass transfer in the weld pool for GMAW by using ripple-based modeling

G. WANG, Graduate Student, and P.G. HUANG, Associate Professor, Department of Mechanical Engineering, and Y.M. ZHANG, Associate Professor, Department of Electrical and Computer Engineering, are with the University of Kentucky, Lexington, KY 40506-0108. Contact e-mail: gwang1@engr.uky.edu or gracie_wang@hotmail.com

Manuscript submitted December 10, 2001.

formulation. The transient shape of the droplet is calculated using the fractional volume of fluid (VOF) method,[21] which is shown to be more flexible and efficient than other methods for treating complicated freeboundary configurations. Gravitational force, surface tension force, and electromagnetic force play fundamental roles in the process of droplet growth and detachment. The continuum surface force (CSF) model[22] used in this study eliminates the need for interface reconstruction, simplifies the calculation of surface tension, and enables accurate modeling of fluid flows driven by surface forces. As the welding current generates the electromagnetic force exerted on the pendant drop, it is essential to include the effects of the current with suitable boundary conditions.

II. NUMERICAL SCHEMES

The numerical schemes employed are based on a finite-difference solution of a coupled set of partial differential equations governing unsteady incompressible fluid flow.[17] The two-step projection method[23] is the basic algorithm for solving this set of partial differential equations. Free surfaces are captured by the VOF method.[21] Surface tension of free surfaces is modeled as a localized volume force derived from the CSF model.[22]

A. *Governing Equations*

In order to simplify the numerical model, the physical process is assumed to be axisymmetric, and the material properties are assumed to be constant. The motion of fluid within the drop is governed by the incompressible Navier–Stokes equations (continuity and momentum equations):

$$\nabla \cdot \boldsymbol{v} = 0 \qquad [1]$$

$$\rho \frac{D\boldsymbol{v}}{Dt} = -\nabla p + \nabla \cdot \mathrm{t} + \boldsymbol{F_b} \qquad [2]$$

where ρ is the fluid density, p is the scalar pressure, τ is the viscous stress tensor, and $\boldsymbol{F_b}$ is the body force, which includes the gravitational force and the electromagnetic force.

The basic scheme for the two-step projection method is to break the computation of the governing equations for unsteady incompressible flow [1] and [2] into two steps. Time discretization form of governing equations is given by the following:

$$\textit{Step } 1: \quad \frac{\boldsymbol{v}^* - \boldsymbol{v}^n}{\Delta t} = -(\boldsymbol{v}^n \cdot \nabla)\boldsymbol{v}^n + \frac{1}{\rho^n}\nabla \cdot \tau^n + \boldsymbol{F}_b^n \qquad [3]$$

$$\textit{Step } 2: \quad \left.\begin{array}{l} \dfrac{\boldsymbol{v}^{n+1} - \boldsymbol{v}^*}{\Delta t} = -\dfrac{1}{\rho^n}\nabla p^{n+1} \\ \nabla \cdot \boldsymbol{v}^{n+1} = 0 \end{array}\right\} \Rightarrow$$

$$\nabla \cdot \left(\frac{1}{\rho}\nabla p^{n+1}\right) = \frac{\nabla \cdot \boldsymbol{v}^*}{\Delta t} \qquad [4]$$

In the first step, a velocity field is computed from viscosity, advection, and body forces, *i.e.,* neglecting the influence from the pressure gradient. In the second step, the velocity field is changed under the influence of pressure only. Since the velocity field must satisfy the continuity equation as well, one Poisson equation is obtained for solving the pressure field.

B. *Tracking the Free Surface*

The transient shape of the droplet is calculated using the VOF[21] method, which was pioneered by Hirt and Nichol. This method has been proved to be a powerful tool when dealing with the problem of free surfaces. A detailed discussion of this method can be found in the literature. Its main features are discussed briefly subsequently.

Free surfaces are reconstructed by means of a scalar field $F(\boldsymbol{x}, t)$, where

$$F(\boldsymbol{x}, t) = \begin{cases} 1 & \text{in the fluid} \\ >0, <1 & \text{at the free surface} \\ 0 & \text{at the void} \end{cases} \qquad [5]$$

For incompressible flow, the VOF function might be regarded as the normalization $F(\boldsymbol{x}, t) = \rho(\boldsymbol{x}, t)/\rho_f$, where ρ_f is the constant fluid density. The discontinuity in F is a Lagrangian invariant, propagating according to

$$\frac{dF}{dt} = \frac{\partial F}{\partial t} + (\boldsymbol{v} \cdot \nabla)F = 0 \qquad [6]$$

The discretization form of Eq. [6] contains terms of F fluxes through the faces of the computational cells. The VOF method is based on the use of reconstructed free surface and donor-acceptor differencing to compute fluxes of fluid advected through the cell faces. The free surface is reconstructed either horizontally or vertically in a surface cell, depending upon its slope obtained from the value of F in neighboring cells. The position of a free surface depends upon the value of F. A donor-acceptor differencing is identified by the direction of the velocity.

C. *Modeling of Surface Tension*

Surface tension at a free surface is modeled with a localized volume force prescribed by the CSF model.[22] Instead of a surface tensile force or a surface pressure boundary condition applied at a discontinuity, a volume force acts on fluid lying within finite thickness transition regions continuously. Surface tension modeled with the continuum method eliminates the need for interface reconstruction, and can be easily calculated by applying an extra body force in the momentum equation.

In its standard form, the surface tension force per unit interfacial area is

$$\boldsymbol{F}_{sa}(\boldsymbol{x}_s) = \sigma\kappa(\boldsymbol{x}_s)\hat{\boldsymbol{n}}(\boldsymbol{x}_s) \qquad [7]$$

It can be reformulated as a volume force by satisfying Green's theory:

$$\lim_{h\to 0}\int_{\Delta V} \boldsymbol{F}_{sv}(\boldsymbol{x})\,dV = \int_{\Delta S} \boldsymbol{F}_{sa}(\boldsymbol{x}_s)\,dS \qquad [8]$$

The volume force $\boldsymbol{F}_{sv}$ is identified as

$$\boldsymbol{F}_{sv}(\boldsymbol{x}) = \sigma\kappa(\boldsymbol{x})\nabla F(\boldsymbol{x})g(\boldsymbol{x}) \qquad [9]$$

The free surface curvature κ follows from the expression

$$\kappa = -(\nabla\cdot\hat{\boldsymbol{n}}) = \frac{1}{|\boldsymbol{n}|}\left[\left(\frac{\boldsymbol{n}}{|\boldsymbol{n}|}\cdot\nabla\right)|\boldsymbol{n}| - (\nabla\cdot\boldsymbol{n})\right] \qquad [10]$$

where

$$\boldsymbol{n} = \nabla F \qquad [11]$$

For incompressible flow, $g(\boldsymbol{x})$ is given by

$$g(\boldsymbol{x}) = 2F(\boldsymbol{x}) \qquad [12]$$

With this option, better results are obtained because the application of the volume force in Eq. [9] does not cause expansion and compression of the transition region.[22]

D. *Calculation of Electromagnetic Force*

The effect of welding current on the metal transfer includes its determination for the electromagnetic force, which is part of the body force in the momentum Eq. [2]. The electromagnetic force generated by the welding current and self-induced magnetic field is expressed as

$$\boldsymbol{F}_m = \boldsymbol{J}\times\boldsymbol{B} \qquad [13]$$

where the self-induced magnetic field is derived from Ampere's law:

$$B_\theta = \frac{u_0}{r}\int_0^r J_z r\,dr \qquad [14]$$

and the current density is calculated from the Ohm's law:

$$J_r = -\sigma\frac{\partial V}{\partial r}, \qquad J_z = -\sigma\frac{\partial V}{\partial z} \qquad [15]$$

Assuming the electric field is quasi-steady-state and the electrical conductivity is constant, the electric potential, being the only unknown variable, can be calculated by solving current continuity equation:

$$\frac{1}{r}\frac{\partial}{\partial r}\left(r\frac{\partial V}{\partial r}\right) + \frac{\partial^2 V}{\partial z^2} = 0 \qquad [16]$$

E. *Boundary Conditions*

Schematic sketches of metal transfer process in GMAW with initial and boundary conditions are shown in Figure 1.

(1) The input velocity of molten metal is assumed to be the same as the wire feed rate.
(2) The problem is assumed to be axisymmetric. Hence, the calculation domain is taken as one side of centerline.
(3) Free slip at the solid boundaries.
(4) Momentum transfer from plasma to the droplet is neglected; the velocities of the surrounding gas are specified by setting them to zero.

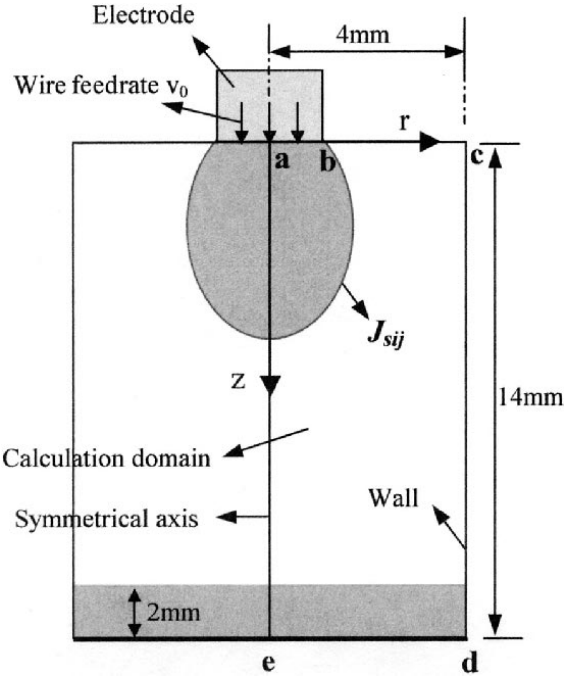

(*a*)

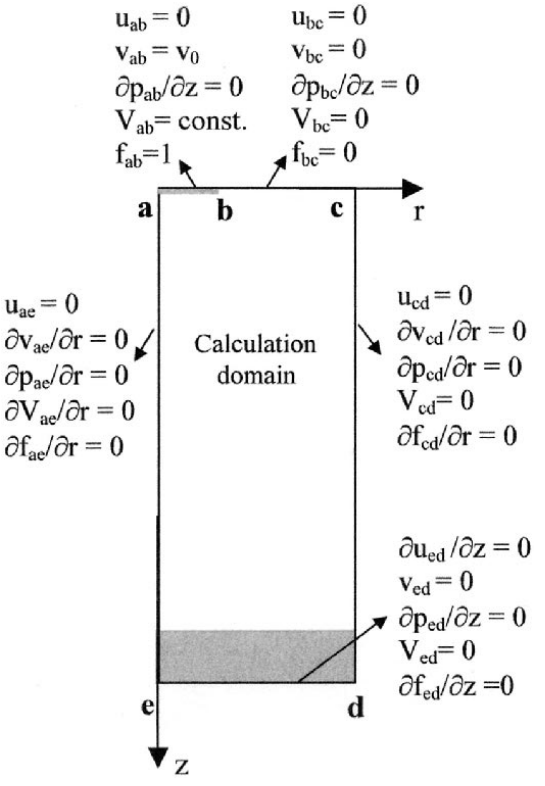

(*b*)

Fig. 1—Schematic sketch of metal transfer process in GMAW with initial and boundary conditions: (*a*) a schematic of metal transfer process and (*b*) initial and external boundary conditions.

(5) The effects of pressure variations in the surrounding gas have been neglected by setting the pressure to atmospheric conditions.

The boundary conditions for solving the Laplace equation to determine the distributions of the potential and current density within the drop, and thus, the influence of the electromagnetic force are

(1) an isopotential line ($\Phi = 0$) is set at the inlet section,
(2) there is symmetry about the centerline,
(3) the current density distribution on the drop surface cell (i, j) is assumed as

$$J_{sij} = I \cdot f(i, j) \Big/ \sum_n (S_{ij} \cdot f(i, j)) \qquad [17]$$

where J_{sij} represents the current density on the surface cell (i, j), I the welding current and S_{ij} the surface area of the free surface cell (i, j). The distribution function $f(i, j)$ is difficult to determine, since there is no experimental measurement of the current density on a GMAW drop surface available in the literature due to the difficulty of making such measurements in the free surface of a drop. The two kinds of current density distribution assumed in the early study by Chio *et al.*[15] are as follows:

$$\text{Uniform current density distribution: } f(i, j) = 1 \qquad [18]$$

$$\text{Linear current density distribution: } f(i, j) = z_j \qquad [19]$$

where z_j represents the distance between the free surface cell (i, j) and solid-liquid interface of the electrode. The calculated results were in broad agreement with the experimental data and suggested that the assumption of the linear current density predicted the experimental results more accurately than the uniform current density. But the transition current is not captured quite accurately using these two current density distribution models.

In this work, a Gaussian current density distribution on the drop surface is proposed:

$$f(i, j) = \frac{1}{\sqrt{2\pi}} \exp(-\xi^2/2) \qquad [20]$$

$$\xi = \frac{X}{D}$$

where X is the arc (curve) length on the drop surface between the lowest point on the drop and the free surface cell (i, j), and D is the diameter of the electrode. The assumption is proposed based on the current density distribution over the workpiece, on which a Gaussian distribution has been detected by previous experiments.[1]

III. RESULTS AND DISCUSSION

Results are presented for the physical model based on the work of Kim and Eagar.[24] Simulations are carried out for a mild steel electrode with 1.6-mm diameter and a feed rate of 70 mm/s. The welding current varies from 150 to 320 A, which covers the range of globular and spray metal transfer. The material properties taken from the work of Chio *et al.*[15] are listed in Table I. The calculations are performed using different assumptions of current density distribution over drop surface, as mentioned previously. A uniform computational mesh with mesh spacing of 0.1 mm in each coordinate direction is used. The time-step is adjusted according to the linear stability constraints. While the mesh spacing was varied between 0.08 and 0.16 mm, it was found that the predicted average drop sizes remain unchanged. Although the change of mesh spacing leads to a change on the details of predicted results in the transition current range (between 230 and 260 A), the averaged sizes were found to be almost the same. All calculations are executed on a SGI-Origin-2100 workstation (Silicon Graphics, Inc.).

Table I. Material Properties of the Electrode

Mass density ρ	7860 kg/m^3
Kinematic viscosity ν	2.8×10^{-7} m^2/s
Surface tension coefficient γ	1.2 N/m
Electrical conductivity σ	8.54×10^5 mho/m
Permeability μ	$4\pi \times 10^{-7}$ H/m

Figures 2 through 4 show the metal transfer processes under the assumption of Gaussian current density distribution for welding currents of 160, 300, and 250 A, respectively. These cases represent the globular transfer with large drops in the low current range, the streaming spray transfer with very small drops in the higher current range, and the transition from the globular to spray transfer with nonuniform drops in a narrow transition current range.

Figure 2(a) shows the profiles for droplet developing at a current of 160 A. The vibration of the drop can be observed at the beginning of the drop formation due to the influence of electromagnetic forces. The drop grows at the tip of the electrode with a classic pendant drop shape, due to gravity and surface tension in the presence of decreasing electromagnetic force. Drop detachment occurs after the neck shrinks. The drop detachment period is about 320 ms. The diameter of detached drops is about 4.4 mm with slight variations. It took 32 hours of CPU time to simulate about 1.6 seconds of real time process.

Figure 2(b) shows the details of calculated potential and velocity distributions within the droplet for the selected instant of time at a current of 160 A. The current density and electromagnetic force are determined by the potential distribution. The current direction (marked in the figure) is vertical to the curve of potential contour and points to the low potential. The magnitude of current density calculated from the gradient of potential depends on the distance between contours of potential with the same value. Different regions with concave contour and convex contour for potential distribution are identified. The current diverges and the electromagnetic force with a downward component arises in the region with concave contours of potential distribution. The current converges and the electromagnetic force with an upward component arises in the region with convex contours of potential distribution.

There are two distinguishing regions with concave potential contour upside and convex potential contour downside observed before the neck forms in Figure 2(b). At $t = 45$ ms, the electromagnetic force dominates the drop behavior compared to the gravitational force. The upside flow driven down by the electromagnetic force with downward component collides with the downside flow driven up by the electromagnetic force with upward component. There is a counterclockwise vortex and a clockwise vortex formed. The competition between the two streams causes the observed vibration of the droplet. The magnitude of the current density decreases with the increase of pendant drop size, according to the observation of the enlargement in distance between contours with the same value. Hence, the gravitational force dominates the flow instead of the

electromagnetic force as the drop becomes larger. The upside flow driven downward by gravitational force and electromagnetic force overcomes the downside flow driven upward by electromagnetic force. Eventually, the electromagnetic force with an upward component can no longer compete with the gravitational force and the flow is driven down to hit the bottom of the drop. There is another region with convex potential contour developed above the neck after it forms in the drop. The flow driven up by the electromagnetic force with the upward component forms a clockwise vortex above the neck. From the distribution of the potential, the electromagnetic force accelerates the drop detachment after the neck shrinks not only as an inward pinch force but also as a detaching force.

Figure 3(a) shows the profiles for droplet developing at a current of 300 A. The electromagnetic force dominates the droplet detachment process compared to the gravity. The drops become much smaller and the drop detachment frequency is much greater. The average drop detachment period is about 3.3 ms with a drop diameter of 0.96 mm. It took 30 hours of CPU time to simulate about 0.2 seconds of real time process.

Figure 3(b) shows the details of the distributions of the calculated potential and velocity within the droplet for a selected instant of time at a current of 300 A. There are two distinct regions with convex contour up and concave contour down in the observed potential distribution. A clockwise vortex and a counterclockwise vortex are induced by the electromagnetic force with an upward component and a downward component, respectively. The current density is very high within the drop compared to the 160 A case. The electromagnetic force dominates the behavior of flow compared to the gravitational force. The surface tension cannot compete with the electromagnetic force before the drop grows larger. The small drop is detached by the electromagnetic force pinching inward and pulling apart.

Figure 4(a) shows the profiles for droplet developing at a current of 250 A. The gravitational force and electromagnetic force both affect the droplet detachment process in the middle of the transition from globular to spray mode. The electromagnetic force helps generate a series of small drops. However, the electromagnetic force is not large enough to detach the entire drop and excess fluid accumulates on the tip of the electrode. The electromagnetic force becomes weaker as this excess fluid drop grows. When enough fluid accumulates at the tip of the electrode, the electromagnetic force will not be able to detach the droplet fluid. A large drop forms and is finally detached by the gravitational force. Hence, a bifurcation in the drop detachment frequency and the drop size is captured by the calculation. There is a large drop formed and detached between every few small drops. The phenomena are consistent with the experimental observation in previous studies.[2] It took 46 hours of CPU time to simulate about 1 second of real time process.

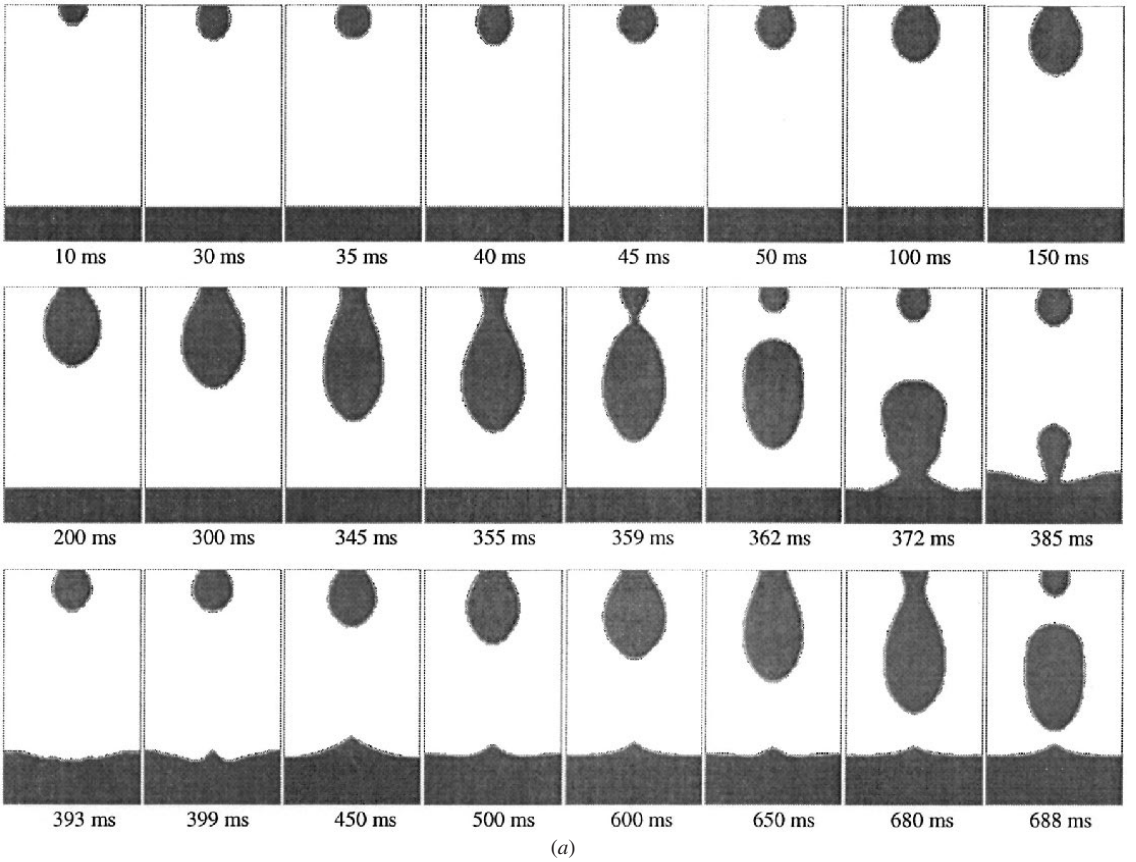

Fig. 2—Metal transfer process at the current of 160 A: (*a*) drop profiles and (*b*) potential and velocity distributions within the droplet.

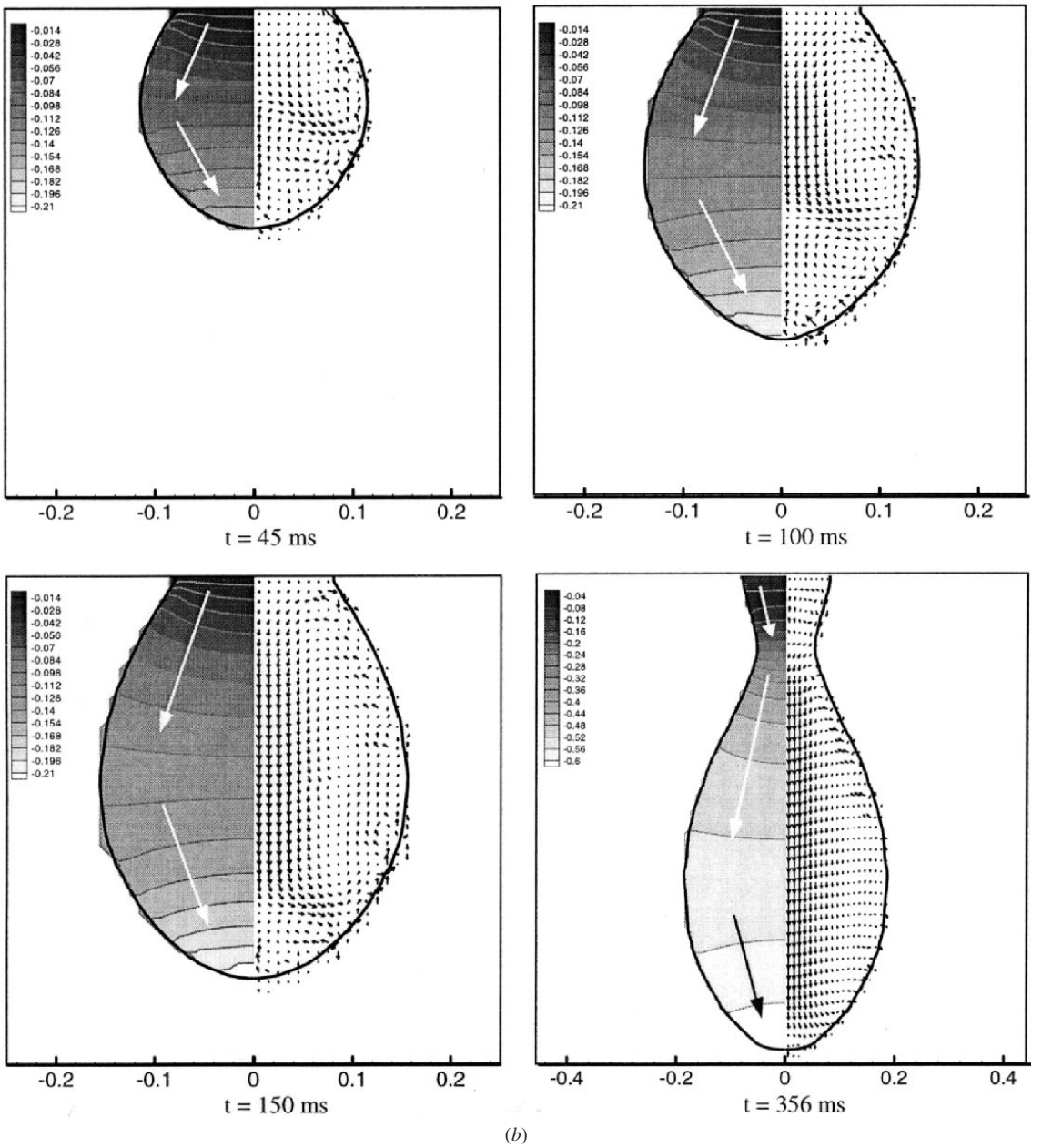

(*b*)

Fig. 2—(continued) Metal transfer process at the current of 160 A: (*a*) drop profiles and (*b*) potential and velocity distributions within the droplet.

Figure 4(b) shows the detail of instantaneous potential and velocity distributions within the droplet for the 250 A case in the middle of transiting from globular to spray mode. A small drop forms on the tip of the electrode with the similar potential and velocity distributions as the 300 A case, while a large drop forms with the potential and velocity distributions similar to when the current is at 160 A.

The predicted average drop sizes by using Gaussian current density distribution over the drop surface for different welding currents are shown in Figure 5. They are compared with the experimentally measured data[24] as well as the results calculated from assuming constant and linear current density distributions. As seen in Figure 5, the average measured drop size decreases with increasing welding current. There exists a transition current range from 230 to 260 A, over which a significant change in the drop size occurs and the metal transfer mode changes from the globular to spray. The images captured in early studies also showed irregularity in droplet sizes distribution in the transition from globular to spray mode. The predicted results by using a Gaussian current density distribution show better agreement with the experimental data than the results obtained using a constant or linear assumption. In particular, the transition current range and the behavior of drop development in this zone are predicted very accurately by using the Gaussian current density distribution assumption.

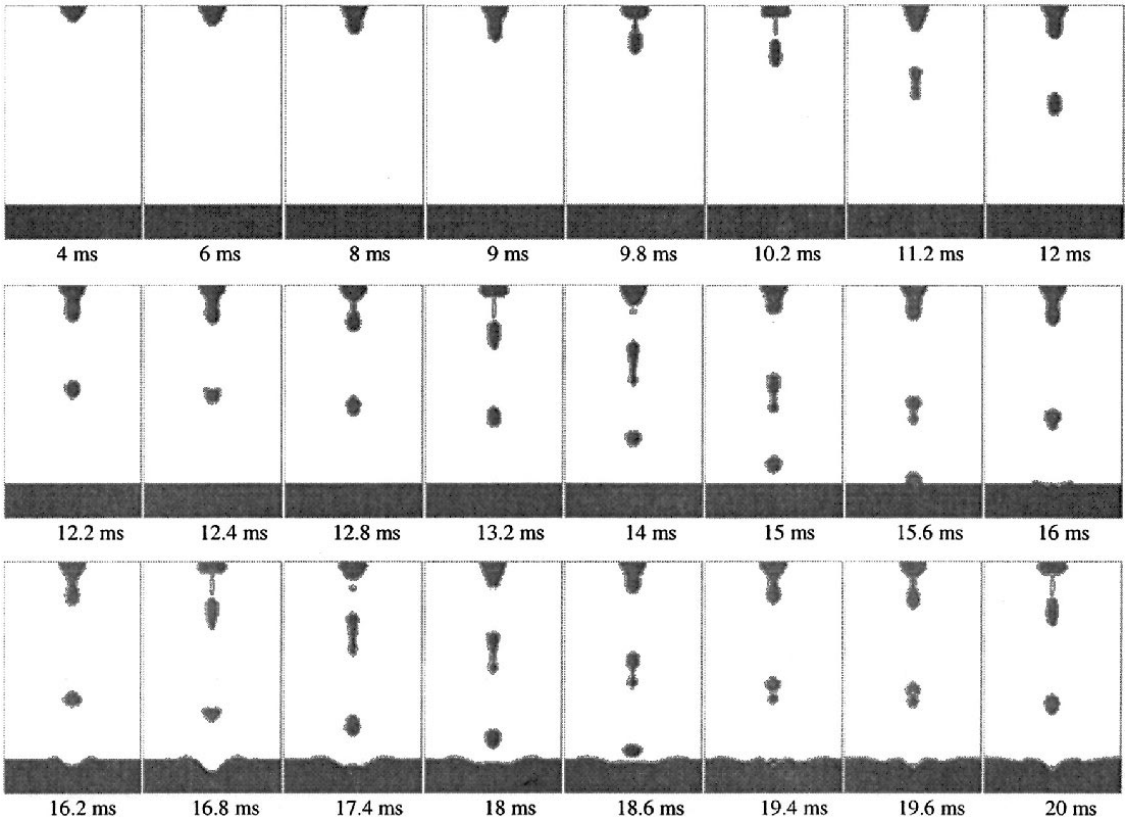

(*a*)

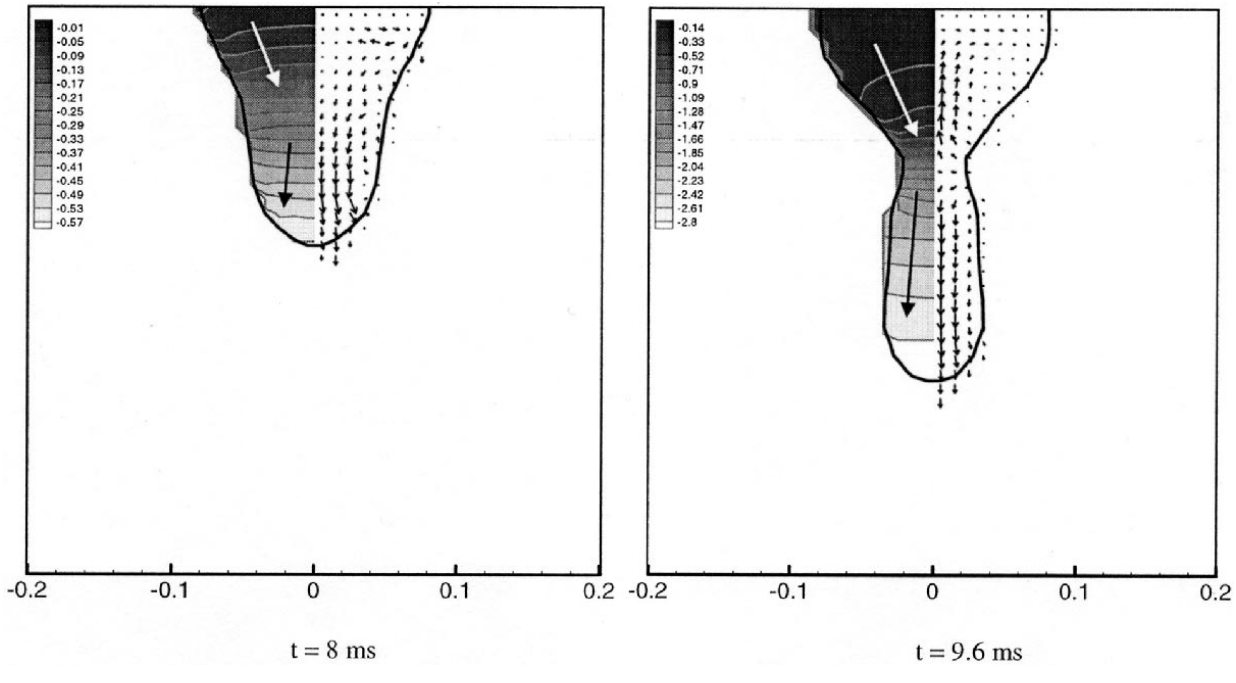

(*b*)

Fig. 3—Metal transfer process at the current of 300 A: (*a*) drop profiles and (*b*) potential and velocity distributions within the droplet.

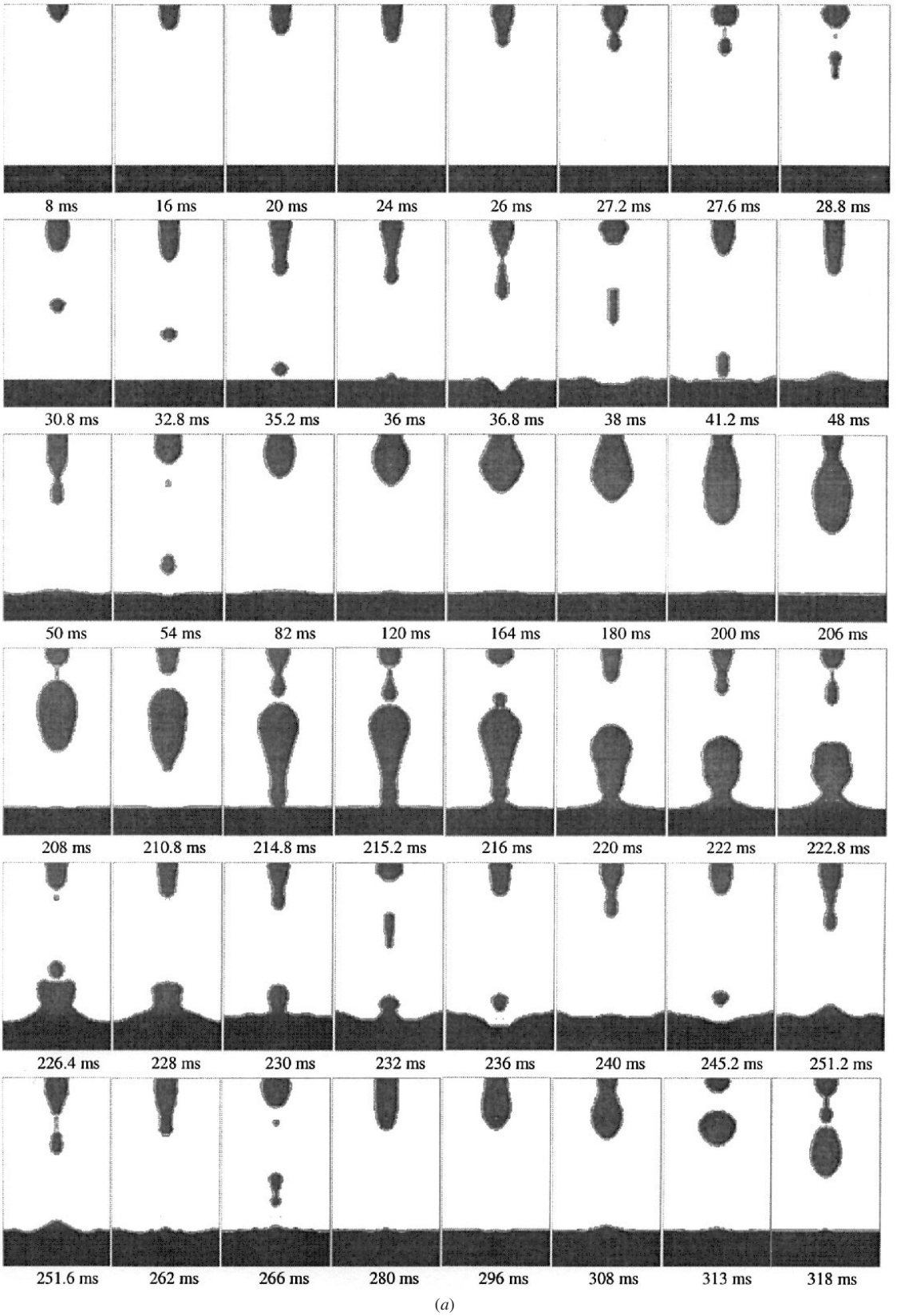

(*a*)

Fig. 4—Metal transfer process at the current of 250 A: (*a*) drop profiles and (*b*) potential and velocity distributions within the droplet.

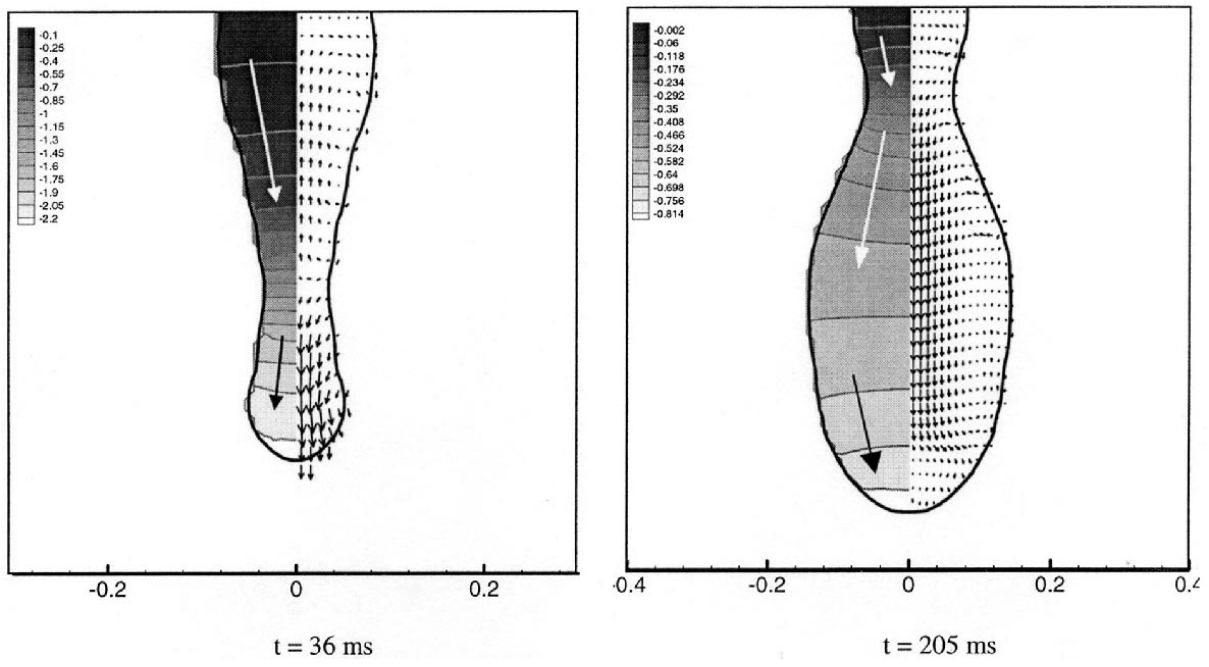

(*b*)

Fig. 4—(continued) Metal transfer process at the current of 250 A: (*a*) drop profiles and (*b*) potential and velocity distributions within the droplet.

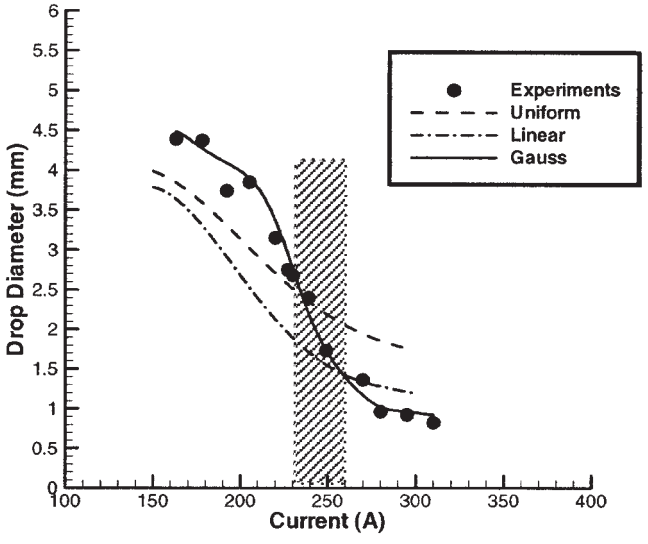

Fig. 5—Comparison of predicted average droplet sizes with experimental results.

IV. CONCLUSIONS

A numerical method employing advanced techniques in CFD has been applied to simulate the dynamic process of metal transfer in GMAW. In the current simulation, effects of the surface tension, electromagnetic, and gravitational forces are considered. The assumption of Gaussian current density distribution on the droplet surface is proposed and shown to provide a very good agreement with the experimental data. The current study provides a good understanding of the physical mechanisms that dominate the metal transfer process under different current ranges in GMAW. The simulation tool will become useful in developing other novel experimental techniques to achieve high-quality welding in GMAW.

ACKNOWLEDGMENT

This work is supported by the Center for Robotics and Manufacturing Systems, University of Kentucky.

REFERENCES

1. J.F. Lancaster: *The Physics of Welding,* 2nd ed., Pergamon Press, Oxford, 1986.
2. L.A. Jones, T.W. Eagar, and J.H. Lang: *Welding J.,* 1998, vol. 77, pp. 135s–41s.
3. A. Lesnewich: *Welding J.,* 1958, vol. 37, pp. 418s–425s.
4. S.W. Simpson, P. Zhu, and M. Rados: *Proc. 42nd Nat. Welding Conf.,* 1994, vol. 31, pp. 1–8.
5. J.H. Waszink and L.H.J. Graat: *Welding J.,* 1983, vol. 62, pp. 109s–16s.
6. J.C. Amson: *Br. J. Appl. Phys.,* 1965, vol. 16, pp. 1169–79.
7. C.J. Allum: *J. Phys. D,* 1985, vol. 18, pp. 1431–46.
8. C.J. Allum: *J. Phys. D,* 1985, vol. 18, pp. 1447–68.
9. V.A. Nemchinsky: *J. Phys. D,* 1994, vol. 27, pp. 1433–42.
10. T.M. Joo, C.D. Yoo, and T.S. Lee: *J. Manu. Sci. Eng.,* 1996, vol. 118, pp. 623–27.
11. S.W. Simpsom and P. Zhu: *J. Phys. D,* 1995, vol. 28, pp. 1594–600.
12. J. Haidar and J.J. Lowke: *J. Phys. D,* 1996, vol. 29, pp. 2951–60.
13. J. Haidar: *J. Phys. D,* 1998, vol. 31, pp. 1233–44.
14. H.G. Fan and R. Kovacevic: *Metall. Mater. Trans. B,* 1999, vol. 30B, pp. 791–801.
15. S.K. Chio, C.D. Yoo, and Y.S. Kim: *Welding J.,* 1998, vol. 77, pp. 38s–44s.
16. S.K. Chio, Y.S. Kim, and C.D. Yoo: *J. Phys. D,* 1999, vol. 32, pp. 326–34.
17. D.B. Kothe, R.C. Mjolsness, and M.D. Torrey: RIPPLE, Los Alamos National Laboratory, Los Alamos, NM, 1994, LA-12007-MS.
18. Y. Wang, H.L. Tsai, S.P. Marin, and P.C. Wang: *Proc. IMECE* '02, ASME Int. Mechanical Engineering Congr. Exp. NO, LA, Nov. 17–22, 2002.
19. Y. Wang and H.L. Tsai: *Int. J. Heat Mass Transfer,* 2001, vol. 44, pp. 2067–80.
20. Y. Wang and H.L. Tsai: *Metall. Mater. Trans. B,* 2001, vol. 32, pp. 501–15.
21. C.W. Hirt and B.D. Nichols: *J. Comp. Phys.,* 1981, vol. 39, pp. 201–25.
22. J.U. Brackbill, D.B. Kothe, and C. Zemach: *J. Comp. Phys.,* 1992, vol. 100, pp. 335–54.
23. F.H. Harlow and J.E. Welch: *Phys. Fluids,* 1965, vol. 8, pp. 2182–90.
24. Y.S. Kim and T.W. Eagar: *Welding J.,* 1993, vol. 72, pp. 269–78.